Probabilistic characteristics analysis for the time-dependent deformation of clay soils due to spatial variability

Feiyang Wang[1,2a], Hongwei Huang[1*], Zhenyu Yin[3b] and Qiang Huang[4c]

[1]Key Laboratory of Geotechnical and Underground Engineering of Ministry of Education, Department of Geotechnical Engineering, College of Civil Engineering, Tongji University, Shanghai, China;
[3]Department Department of Civil and Environmental Engineering, The Hong Kong Polytechnic University, Hung Hom, Kowloon, Hong Kong, China;
[4]Institute of geotechnical engineering, Ningbo University, Ningbo, China

Abstract. Consolidation and creep are two types of time-dependent deformation of clay soil. However, the soil deformation presents probabilistic behaviors when the spatial variability is considered. The Monte-Carlo method is used to sample anisotropic random fields that are mapped into two-dimensional random finite element models (RFEM) to analyze the influences of spatial variability on the time-dependent deformation of clay soil. The anisotropic random fields of soil parameters are generated by a spectral representation method (SRM) to describe the spatial variability of clay soil. The consolidation and the creep problems are modeled by Biot's consolidation theory and the creep model proposed by Yin *et al.* (2010) respectively. The spatial variability of Young modulus and permeability coefficient in probabilistic consolidation analysis and the secondary consolidation coefficient in probabilistic creep analysis are emphasized by the RFEM simulation. The results show that the scale of fluctuation (SOF)

∗Corresponding author, Professor, E-mail: huanghw@tongji.edu.cn
[a] Ph.D. Student, E-mail: feiyang.wong20@gmail.com
[b] Professor, E-mail: zhenyu.yin@polyu.edu.hk
[c] Ph.D., E-mail: qianghuang1987@163.com

in vertical direction and the coefficient of variation (COV) of Young modulus and permeability have significant influences on the probabilistic characteristics of consolidation behavior. Besides, the bunched region of low permeability soil produces a blockage effect, which seriously affects the consolidation characteristics. It is found that the uncertainty of creep deformation will accumulate over time until it remains constant. The variability of creep deformation increases with the increase in the vertical SOF and COV of the secondary consolidation coefficient. The research also provides insightful clues for the time-varying reliability design related to the time-dependent deformation of clay soil.

Keywords: clay soil; time-dependent deformation; spatial variability; blockage effect; scale of fluctuation; horizontally stratified anisotropic random field

1. Introduction

Due to the rapid development of infrastructure engineering, it is increasingly common to construct road embankments and other geotechnical structures. However, there is an obvious time-dependent deformation when these projects are constructed on clay soil. For example, Morsy *et al.* (1995) have reported that the movements of a dike monitored are over 1 m due to the time-dependent deformation of a clay soil layer for more than 25 years. The spatial variability is usually numerically reconstructed with random field theory. Papaioannou and Straub (2012) simulated the soil with a homogeneous random field to analyze the structural reliability of a pile wall. Chenari *et al.* (2019) used heterogeneous random fields to perform numerical simulations on the samples to explain the physical variability of the soil. In geotechnical engineering sites, soil is often isotropic in horizontal direction. Therefore, it is necessary to adopt a horizontally stratified anisotropic random field to investigate the effects of spatial variability on the time-dependent deformation of clay soil.

Clay soils are characterized by remarkable time-dependent behaviors including consolidation and creep. The former is well dealt with the widely used Biot's consolidation theory (Biot 1941), while for the latter elastic-visco-plastic (EVP) models effectively and accurately predict creep deformation (Karim and Gnanendran 2014). However, most of the EVP models are hard to be used by geotechnical engineers due to complicated formulations and numerous parameters. Yin *et al.* (2010) have proposed an EVP model, which is based on the widely-used and comprehensible modified Cam-Clay model (MCCM). The proposed model can predict creep behaviors of clay soils well. In the isotropic case, there is only one additional parameter, the secondary consolidation coefficient $C_{\alpha e}$, compared to MCCM.

Although Biot's consolidation theory and the EVP model proposed by Yin *et al.* (2010) are available to predict the time-dependent deformation, it is still difficult to accurately predict the deformation of clay soils on site without involving the spatial variability of soil parameters. The variability of soil mainly comes from its inherent variability and test errors due to the geologic investigation (Bárdossy and Fodor 2001). The former which is focused in this paper is described as an anisotropic random field based on statistical parameters of soil. Young modulus, permeability, and secondary consolidation coefficient are significant parameters for estimating the time-dependent deformation. The random field characterized by the coefficient of variation (COV) and the scale of fluctuation (SOF) is an effective tool to represent the spatial variability of these parameters (Vanmarcke 2010). The SOF is determined by a large amount of laboratory or in-situ tests. To overcome this obstacle, Fei *et al.* (2019) proposed a numerical simulation method based on soil microstructure to calculate the SOF.

Lee *et al.* (1983) have summarized that the COV of the Young modulus ranges from 2% to 42%. The COV of the permeability for a specific soil is relatively large, ranging from 60% to 200% as

reported by Zhang *et al.* (1974). Benson (1993) has analyzed the permeability of the clay soil collected from 57 landfills. The COV of permeability ranges from 27% to 300%, and most of the data follow lognormal distribution. The secondary consolidation coefficient $C_{\alpha e}$ of clay soil has been investigated by Xu *et al.* (2008), where $C_{\alpha e}$ varies from 0.0056 to 0.0066, and the COV ranges from 0.2 to 0.4. As for the SOF, there is a large difference between the vertical and horizontal directions. The SOFs in these two directions are in the range of 2~6m and 20~80m respectively (Rehfeldt *et al.* 1992, Prevost *et al.* 1997, Phoon and Kulhawy 1999).

Many relevant researchers have studied the influence of spatial variability of soils on deformation. Kim *et al.* (2012) employed ordinary kriging and three theoretical semivariograms models to estimate the spatial distributions of geo-layers, and then to evaluate the uncertainty in spatial distributions of consolidation settlement. Probabilistic settlement of spread footing on spatial variability of Young modulus has been estimated by using a two-dimensional random finite element model (RFEM), in which the spatial variability is described by the random field generated by local average subdivision (Fenton and Griffiths 2002). In the study of time-dependent deformation of clay soils, the influence of the spatial variation on one-dimensional consolidation has been evaluated using a stochastic approach (Li and Hu 2011). By using a first-order reliability method (FORM) and stochastic response surface method (SRSM), Bong and Stuedlein (2018) maintained that the variability of average consolidation degree increases as the SOF increases. However, the probabilistic characteristics of time-dependent deformation, especially the creep of clay soils, have not been systematically studied.

RFEM has been an effective and rigorous method to simulate ground responses considering spatial variation. The main disadvantage of RFEM is time-consuming (Schueller 1997). With the great progress of high-performance computers, computational efficiency has been greatly improved. As a stochastic approach, RFEM is employed by mapping the random field into the FE program.

Then, a number of realizations sampled by the Monte-Carlo method are carried out to obtain the concerned time-dependent deformation. In this study, the probabilistic deformations of consolidation and creep are separately solved by RFEM based on Biot's consolidation theory and the model proposed by Yin and Chang *et al.* (2010).

This paper aims to investigate the influences of spatial variability on the time-dependent deformation of clay soils. The outline of this paper is organized as follows. In Section 2, the random field is generated by spectral representation method (SRM) to describe the spatial variability of the soil. Then, the random field is mapped into a commercial finite element software, and RFEM is implemented, which is validated by a case. In Section 3, the spatial variability of clay soil is treated by a horizontally stratified anisotropic random field, and random finite element models for time-dependent deformation are established. In Section 4, the probabilistic characteristics of time-dependent deformation including consolidation and creep are analyzed by using the established random finite element models. The consolidation deformation of RFEM is simultaneously compared with the calculation results of the simplified method.

2. Fundamental of random field and implementation of RFEM

The finite element method (FEM) as a deterministic analysis method is extensively used in simulating the continuous medium in geotechnical engineering. In order to better simulate the uncertain ground response, RFEM is implemented by a number of finite element models coupled with random fields to consider the spatial variability of the field soil. To achieve this purpose, Gaussian stationary random fields are first generated by using a spectral representation method (SRM). RFEM is then realized by mapping the random fields into the commercial program ABAQUS. Eventually, the RFEM is validated by a consolidation case.

2.1 Generation of anisotropic Gaussian stationary random field

The spectral representation method (SRM) has been widely used to generate a discrete Gaussian random field in the spatial domain due to its versatility and robustness. This method was first developed by Bergman and Shinozuka *et al.* (1997) to simulate multidimensional, multivariate and non-stationary random processes or fields. Many works have been carried out to demonstrate the accuracy of this method. The mean value of a random field generated by the SRM is identical to the excepted mean value (Hu and Schiehlen 1997). Additionally, the SRM is not only accurate in terms of cumulative density functions (CDF) or lower order moments but also much faster when compared to the Karhunen-loeve expansion method (Stefanou 2009).

To illustrate the detail of SRM, the generation of a univariate and three-dimensional (1V-3D) anisotropic random field is introduced as follows. Let $V(x, y, z)$ be a 1V-3D anisotropic random field in the spatial domain, whose mean value and power spectral density function (PSDF) are denoted by μ and $S(\omega_1, \omega_2, \omega_3)$, respectively. In the frequency domain, the random field $V(x, y, z)$ is written as Eq. (1) (Vanmarcke 2010). It should be pointed out that the generated random field $V(x, y, z)$ is asymptotically Gaussian as N_1, N_2, and N_3 approach infinity according to the multivariate central limit theorem.

$$V(x,y,z) = \mu + \sqrt{2}\sum_{n_1=0}^{N_1-1}\sum_{n_2=0}^{N_2-1}\sum_{n_3=0}^{N_3-1} A_{n_1 n_2 n_3}\cos\Phi_{n_1 n_2 n_3}\exp\left\{i(\omega_{n_1}x+\omega_{n_2}y+\omega_{n_3}z)\right\} \tag{1}$$

where $A_{n_1 n_2 n_3} = \sqrt{2S(\omega_{n_1},\omega_{n_2},\omega_{n_3})\Delta\omega_1\Delta\omega_2\Delta\omega_3}$, $\Delta\omega_i = \dfrac{\omega_{ui}}{N_i}$. ω_{ui} are the cut-off wave numbers that define the active region of PSDF $S(\omega_1, \omega_2, \omega_3)$. Phase angles $\Phi_{n_1 n_2 n_3}$ are random variables that are mutually independent and uniformly distributed over the interval $(0, 2\pi)$.

As we all known, random field is composed of many spatially related random variables. It is assumed that the random variables in the random field $V(x, y, z)$ obey the Gaussian distribution. According to this assumption, a covariance function $B(x, y, z)$ is written in Eq. (2). The form of $\rho(x, y, z)$ has little influence on the random field (Vanmarcke 2010). The Gaussian correlation function $\rho(x, y, z)$ in Eq. (3) is adopted in this study. Here, θ denotes the scale of fluctuation (SOF). By substituting Eqs. (2) and (3) into the transformation formula Eq. (4), it is easy to estimate the PSDF $S(\omega_1, \omega_2, \omega_3)$. The scale of fluctuation (SOF) θ, mean value μ and standard deviation σ are the fundamental parameters of the random field $V(x, y, z)$. These parameters are usually estimated through the field test (Phoon and Kulhawy 1999). Finally, the random field $V(x, y, z)$ can be conveniently calculated by Eq.(1).

$$B(x,y,z) = \sigma^2 \rho(x,y,z) \tag{2}$$

$$\rho(x,y,z) = \mathrm{e}^{-\pi(x^2+y^2+z^2)/\theta^2} \tag{3}$$

$$\begin{cases} B(x,y,z) = \int_{-\infty}^{+\infty}\int_{-\infty}^{+\infty}\int_{-\infty}^{+\infty} S(\omega_1,\omega_2,\omega_3)\cos(\omega_1 x+\omega_2 y+\omega_3 z)d\omega_1 d\omega_2 d\omega_3 \\ S(\omega_1,\omega_2,\omega_3) = (\frac{1}{2\pi})^3 \int_{-\infty}^{+\infty}\int_{-\infty}^{+\infty}\int_{-\infty}^{+\infty} B(x,y,z)\cos(\omega_1 x+\omega_2 y+\omega_3 z)dxdydz \end{cases} \tag{4}$$

Although the Direct Fourier Transform (DFT) can be employed to convert from the spatial domain to the frequency domain with Eqs. (2) and (4), this method is time-consuming due to the heavy computation. Therefore, a Fast Fourier Transform (FFT) technique based butterfly algorithm proposed by Cooley and Tukey (1965) is applied to dramatically improve computational efficiency. In order to take advantage of FFT, Eq. (1) is rewritten as Eq. (5).

158
$$V(m_1\Delta x, m_2\Delta y, m_3\Delta z) = \mu + (\sqrt{2})^3 \,\mathrm{Re}\left\{\sum_{n_3=0}^{N_3-1}\mathrm{Re}\left\{\sum_{n_2=0}^{N_2-1}\mathrm{Re}\left\{\sum_{n_1=0}^{N_1-1} A_{n_1 n_2 n_3}\exp(i\Phi_{n_1 n_2 n_3})\exp(i\frac{2\pi}{N_1}n_1 m_1)\right\}\right.\right.$$
$$\left.\left.\exp(i\frac{2\pi}{N_2}n_2 m_2)\right\}\exp(i\frac{2\pi}{N_3}n_3 m_3)\right\},\quad m_i = 0,1,...,N_i - 1 \tag{5}$$

159 where Re denotes the real part of the complex number.

160 Additionally, to ensure the ergodicity of the random field, the relative error ε in Eq. (6) is set to
161 a small value, and then suitable cut-off wave numbers ω_{ui} are estimated. The relative error ε is an
162 important parameter to ensure the accuracy of random field (Hu and Schiehlen 1997). After
163 estimating of ω_{ui}, the PSDF $S(\omega_1, \omega_2, \omega_3)$ is calculated by Eqs. (2) and (4), and the random field is
164 eventually generated by Eq. (5).

165
$$\int_0^{\omega_{1u}}\int_0^{\omega_{2u}}\int_0^{\omega_{3u}} S(\omega_1,\omega_2,\omega_3)d\omega_1 d\omega_2 d\omega_3 = (1-\varepsilon)\int_0^{+\infty}\int_0^{+\infty}\int_0^{+\infty} S(\omega_1,\omega_2,\omega_3)d\omega_1 d\omega_2 d\omega_3 \tag{6}$$

166

167 *2.2 Implementation of RFEM*

168 In the probabilistic analysis, each RFEM realization is coupled with a random field sampled by
169 the Monte-Carlo method. In this process, a number of random fields of soil parameters based on
170 SRM are firstly generated by a small in-house program. Then, the random fields are separately
171 mapped into the established finite element model. The entire process in this study is developed by
172 Python and the commercial finite element program ABAQUS. To ensure the success of each RFEM,
173 there are two basic prerequisites: one is that the random variable in each random field takes a non-
174 negative value, and the other is that the random variable can represent the statistics over a specific
175 mesh domain.

176 As mentioned above, the Gaussian correlation function Eq. (3) is substituted into Eq. (4) to
177 calculate the PSDF, and the Gaussian stationary random field in the spatial domain is generated by

using Eq. (5). In order to satisfy the first prerequisite, an assumption is made that the concerned parameter X follows a lognormal distribution. The random variable X follows a lognormal distribution, which is characterized by the mean value μ_X, standard deviation σ_X, and SOF $\theta_{\ln X}$. The mean value $\mu_{\ln X}$ and standard deviation $\sigma_{\ln X}$ of $\ln X$ are given by the following formulas.

$$\sigma_{\ln X}=\sqrt{\ln[1+(\sigma_X/\mu_X)^2]} \tag{7}$$

$$\mu_{\ln X}=\ln\mu_X-0.5\sigma^2_{\ln X} \tag{8}$$

As for the second prerequisite, the variance reduction is needed to be taken into account by using a local average method. The reason for the decrease in variance is that the point variance of soil parameter is usually obtained from field measured data, but actually, there is a decrease from the point variance to the local variance over the element domain in the mesh. Therefore, a variance function of the local average method shown in Eq. (9) is adopted to consider the reduction effect by the integration of PSDF over the frequency domain.

$$\gamma(T_x,T_y,T_z)=\int_0^{T_x}\int_0^{T_y}\int_0^{T_z}(T_x-x)(T_y-y)(T_z-z)\rho(x,y,z)dxdydz \tag{9}$$

where T_x, T_y and T_z are the sizes of an element in the x, y, and z directions, respectively.

In order to accurately map the random field X into the mesh of the FE model, the standard deviation $\sigma_{\ln X}$ is reduced by Eq. (10) according to the given mesh size.

$$\sigma^2_{\ln\bar{X}}=\gamma(\bar{X})\sigma^2_{\ln X} \tag{10}$$

where the variance function $\gamma(\bar{X})$ is calculated by Eq.(9).

For given statistics of $\ln X$, a standard Gaussian random field $g_{\ln X}$ is generated by the previous process. The standard Gaussian random field $g_{\ln X}$ is then transformed into lognormal random field

198 g_X according to Eq. (11).

199 $$g_X = \exp(\mu_{\ln X} + \sigma_{\ln \bar{X}} g_{\ln X}) \tag{11}$$

200

201 *2.3 Validation of RFEM*

202 A 1-D probabilistic consolidation case is taken as a verification example in this section. This case
203 has been studied by Huang *et al.* (2010), in which the random field is generated by a local average
204 subdivision method proposed by Fenton and Griffiths (2002).

205 The 1-D RFEM is set to be free drainage on the top boundary. The permeability k and
206 compression coefficient m_v are all assumed to follow the lognormal distribution. The mean values
207 of these parameters are equal to 1.0, and the COVs are equal to 0.5. The scale of fluctuations (SOFs)
208 of permeability and compression coefficient, $\theta_{\ln k}$ and $\theta_{\ln m_v}$, are all equal to 1.0. The cross-correlation
209 coefficient between the permeability k and the compression coefficient m_v is assumed to be 1.0.

210 The equivalent consolidation coefficient defined by the log-time method (Casagrande 1936) is
211 written as follows.

212 $$C_{t50} = \frac{0.197H^2}{t_{50}} \tag{12}$$

213 $$\begin{cases} U_{avs} = \dfrac{S_t}{S_u} \\ U_{avp} = 1 - \dfrac{1}{H}\displaystyle\int_0^H \frac{u}{u_0} dh \end{cases} \tag{13}$$

214 where H is the thickness of the consolidation soil, S_t and S_u are the deformations at time t and
215 complete consolidation, respectively, u and u_0 are the pore pressures at time t and initial time, and
216 t_{50} is the consolidation time when the average consolidation degree U_{avs} or U_{avp} is equal to 50%. In

Eq. (13), U_{avs} and U_{avp} are defined by settlement and excess pore pressure, respectively. The corresponding equivalent consolidation coefficients C_{t50s} and C_{t50p} at time t_{50} can be calculated by Eq. (12).

Regarding the permeability and compression coefficient as random fields, a lot of RFEM simulations are carried out based on the Monte-Carlo method. The equivalent consolidation coefficients are calculated according to Eq. (12). The probability distributions of the equivalent consolidation coefficient are presented in Figs. 1 (a)-(b) $\hat{\mu}$, μ and $\hat{\sigma}$, σ are the mean values and standard deviations of the equivalent consolidation coefficient obtained by RFEM in this study and by Huang *et al.* (2010), respectively. The subscripts *t50s* and *t50p* denote the consolidation times when the average consolidation degrees U_{avs} and U_{avp} are equal to 50%. The histograms calculated by the proposed RFEM are in good agreement with the probability density curves given by Huang *et al.* (2010), in which the relative errors of the mean value and standard deviation are both less than 10%. The results indicate that the proposed RFEM is effective and available to characterize the spatial variability of soil.

3. Random finite element model for time-dependent deformation

3.1 Basic model

There are two main stages of time-dependent behaviors of clay soil, including consolidation and creep. In the first stage, the consolidation induced by drainage is the main cause of soil deformation. When pore pressure remains constant with time or the consolidation is finished, the creep becomes the dominant factor of soil deformation. In order to simulate the time-dependent deformation, Biot's consolidation theory and the creep model proposed by Yin and Chang *et al.* (2010) are respectively used to solve the consolidation deformation and creep deformation in RFEM.

240 Fig. 2 shows the physical schematic of RFEM for calculating the time-dependent deformation.
241 The horizontal and vertical dimensions of the model are $H \times W$. The initial consolidation pressure or
242 pre-consolidation pressure P_0 is applied to the top surface. The free drainage boundary is only set at
243 the top surface. The left and right boundaries are horizontally constrained, and the bottom boundary
244 is fixed in vertical and horizontal displacement.
245 As for an anisotropic random field, the SOFs in vertical and horizontal directions are significant
246 parameters. The ranges of the vertical and horizontal SOFs are generally 2~6m and 20~80m,
247 respectively (Rehfeldt et al. 1992, Prevost *et al.* 1997, Phoon and Kulhawy 1999). Therefore, the model
248 size is determined according to the influence analysis of the SOFs. As shown in Figs. 3 (a)-(c),
249 normalized anisotropic random fields are generated by using the SRM. The results indicate that the
250 anisotropic random field in horizontal direction varies little when the horizontal SOF is in the range
251 of 20~80 m, and the anisotropic random field is approximately homogeneous in horizontal within 5
252 m or less that is 1/4 of the horizontal SOF. In order to ensure the computational efficiency, the width
253 of the model W is set to 1m in the following analysis. In this situation, the generated anisotropic
254 random field is similar to horizontally stratified soil (Huang *et al.* 2017). The horizontally stratified
255 anisotropic random field is adopted here to simulate the spatial variability of soil. The following
256 anisotropic random field refers to the horizontally stratified anisotropic random field.
257 The normalized anisotropic random fields with vertical SOF of 2~6 m are shown in Figs. 4 (a),
258 (b) and (c). The thickness H of the concerned clay soil is 20 m. As shown in Fig. 4, the random field
259 tends to be isotropic with an increase in vertical SOF. The results show that the vertical SOF is an
260 important parameter for the spatial variability of the horizontally stratified soil. Therefore, the
261 vertical SOF is emphasized in the following analysis.
262

263 *3.2 Spatial variability of soil parameters for time-dependent deformation*

264 *3.2.1 Parameters for soil consolidation*

265 The consolidation of clay soil is modeled by RFEM based on Biot's consolidation theory, in
266 which Young modulus E and permeability coefficient k are important mechanical parameters. As
267 mentioned before, soil properties have a great deal of spatial variability. To simplify, Young modulus
268 E and permeability coefficient k are regarded as independent random fields (The cross-correlation
269 coefficient is 0). Under this assumption, the variance of the results is conservative because the
270 permeability is negatively correlated with the Young modulus within the same soil layer (Cho 2010).
271 A deposit soft clay soil is adopted in the probabilistic consolidation analysis. The soft clay in the
272 model is saturated and has high compressibility. The mean value, COV, and SOF of Young modulus
273 E and permeability coefficient k are the basic input parameters of the random finite element model.
274 Relevant studies have shown that the COVs of permeability k and Young modulus E for the clay soil
275 are in the range of 100~300% and 15~30% (Baecher and Christian 2003, Benson 1993). The basic
276 parameters for soil consolidation are listed in Table 1. If there are no special statements, the
277 parameters in the random finite element model are in accordance with Table 1.
278

279 *3.2.2 Parameters for soil creep*

280 As another type of time-dependent deformation of clay soil, the creep behavior is successfully
281 described by the anisotropic EVP model proposed by Yin *et al.* (2010). It should be pointed out that
282 this model is based on the strain rate form of the modified Cam Clay model (MCCM).

283 $$\dot{\varepsilon}_v = \dot{\varepsilon}_v^e + \dot{\varepsilon}_v^{vp} = \frac{\lambda}{\lambda - \kappa}\dot{\varepsilon}_v^{vp} \tag{14}$$

284

where $\dot{\varepsilon}_v^e$ is the elastic strain rate, $\dot{\varepsilon}_v^{vp}$ is the viscoplastic strain rate, λ is the compression index, and κ is the swelling index.

$$\dot{\varepsilon}_v^{vp} = \mu\left(\frac{\sigma_p^{'}}{\sigma_{p0}^{'}}\right)^N \frac{M_c^2 - \eta_{K0}^2}{M_c^2 - \alpha_{K0}^2} \tag{15}$$

where $\mu = \frac{C_{\alpha e}\left(M_c^2 - \alpha_{K0}^2\right)}{\tau\left(M_c^2 - \eta_{K0}^2\right)}$, $N = \frac{\lambda - \kappa}{C_{\alpha e}}$, $\alpha_{K0} = \eta_{K0} - \frac{M_c^2 - \eta_{K0}^2}{3}$, $\eta_{K0} = \frac{3M_c}{6 - M_c}$, M_c is the critical state ratio, $\sigma_p^{'}$ is the initial yield stress, $\sigma_{p0}^{'}$ is the reference pre-consolidation pressure, and τ is the reference time.

Most parameters of this model are the same as MCCM, including compression index λ, swelling index κ, critical state ratio M_c, permeability k, void ratio e_0, pre-consolidation pressure P_0, and Poisson's ratio v. Moreover, there is only one additional parameter, the secondary consolidation coefficient $C_{\alpha e}$, in this EVP model to characterize the creep behavior of clay soil compared to MCCM. These parameters can be estimated from two types of tests, a constant strain-rate oedometer test and a 24h standard oedometer. Researchers interested in the details of this model can refer to the study by Yin *et al.* (2010). The parameters of this creep model for one kind of clay soil are listed in Table 2.

The physical schematic for each RFEM realization is shown in Fig. 2. The saturated clay soil adopted in the RFEM realization is characterized as a low organic content and high plastic with a plastic limit 48% and a liquid limit 90% (Yin *et al.* 2010), and has obvious long-term creep behavior. The creep behavior is modeled with the isotropic form of the EVP model. As observed in the field, the pore pressure changes very little in the creeping stage (Morsy *et al.* 1995). The secondary consolidation coefficient $C_{\alpha e}$ in the creep model is an important factor affecting the time-dependent deformation. Therefore, the spatial variability of the secondary consolidation coefficient $C_{\alpha e}$ should be emphasized in the probabilistic analysis of creep deformation. The $C_{\alpha e}$ of clay soil varies from

0.0056 to 0.0066, and the range of its COV is 0.2~0.4 (Xu *et al.* 2008, Baecher and Christian 2003). In the following analysis, the mean value of C_{ae} takes 0.006, and the range of its COV is 0.2~0.4. Additionally, the horizontal SOF is 40m, and the vertical SOF is within 2~20m.

4. Probabilistic characteristics of time-dependent deformation

Biot's consolidation theory and the creep model proposed by Yin *et al.* (2010) are adopted in RFEM to simulate the time-dependent behavior of clay soil. In the model, the random field obtained by SRM is sampled and mapped into the model. A series of RFEM realizations are carried out by the Monte-Carlo method, and the obtained time-dependent deformations are statistically analyzed.

In order to ensure reliability and efficiency, the number of the RFEM realizations used for consolidation and creep is first determined by the convergence of the standard deviation (Huang *et al.* 2010). In the random finite element model, the concerned parameters of the soil are regarded as independent anisotropic random fields.

4.1 Influence of anisotropic random field on soil consolidation

Soil consolidation is usually accompanied by the dissipation of excess pore pressure. Therefore, the consolidation behavior can be reflected by the average consolidation degree along the thickness of the clay soil, defined by the excess pore pressure, as shown in the second equation in Eq. (13). An ensemble of RFEM realizations with anisotropic random fields of Young modulus and permeability are separately carried out to calculate the possible average consolidation degrees.

To ensure the reliability and efficiency of the proposed RFEM, the sensitivity of the results to the number of Monte-Carlo simulations is checked. The optimal number of RFEM realizations is the minimum number to make the standard deviation of the average consolidation degree σ_U converge.

In the case of the worst convergence, the standard deviation and simulation number curves of two consolidation times are shown in Fig. 5. The horizontal axis represents the number of RFEM realizations, and the vertical axis represents the standard deviation of the average consolidation degree. It can be easily found from the convergence curves that σ_U remains constant when the number of RFEM realizations is greater than 1000. Therefore, the number of RFEM realizations takes 1000 in the following consolidation analysis.

4.1.1 Anisotropic random field of Young modulus

A set of possible average consolidation degrees are obtained from 1000 RFEM realizations with Young modulus as an anisotropic random field. The probability distributions of average consolidation degree at any consolidation time can be estimated for the given vertical SOF $\theta_{\ln E}$ and COV of Young modulus. The following symbols are declared here: μ and σ denote the mean value and standard deviation of the average consolidation degree computed by RFEM, $\hat{\mu}$ and $\hat{\sigma}$ are the statistics estimated by the following analytical method, and the subscripts "vt20" and "vt100" stand for the consolidation time $t = 2\times10^6$ s and $t = 1\times10^7$ s.

Vertical SOF of Young modulus

To illustrate the influence of vertical SOF on the consolidation, the probability distributions of the average consolidation degree around 0.7 at 1×10^7 s are plotted in Fig. 6. The histograms and dotted lines in the figure are obtained by RFEM with various vertical SOFs. With the increase of $\theta_{\ln E}$ from 0.1H to 1.0H, the mean value of the average consolidation degree remains basically unchanged, while the standard deviation increases.

As for an extreme case, the anisotropic random field shown in Figs. 3-4 becomes the same as the

353 $\theta_{\ln E}$ increases to large enough. In this case, the probability distribution calculated by the RFEM is
354 the same as that obtained by FEM with E as a random variable following lognormal distribution.
355 This situation can be reasonably considered as 1-D consolidation, and the average consolidation
356 degree can be solved by using Terzaghi's explicit solution Eq. (16).

357 $$U(t) = P_0 \sum_{m=1}^{\infty} \frac{1}{M^2} e^{-M^2 T_v} \tag{16}$$

358 where $T_v = \frac{C_v t}{H^2} = \frac{kt(1-v)}{\gamma_w H^2 (1-v-2v^2)} E$ and $M = \frac{(2m-1)\pi}{2}$. H is the thickness of soil layer, v is
359 Poisson's ratio, t is consolidation time and P_0 is initial consolidation pressure.

360 Taking Young modulus E as a random variable, the probability density function (PDF) $f(U)$ of
361 average consolidation degree U is derived from Eq. (16).

362 $$f(U) = \frac{E}{2T_v \sum_{m=1}^{\infty} e^{-M^2 T_v}} f(E) \tag{17}$$

363 Moreover, in order to consider vertical SOF, the variance function Eq. (9) is introduced to reduce
364 the standard deviation obtained from Eq. (17). The probability distribution is recalculated according
365 to the reduced standard deviation. The probability distributions for various vertical SOFs are
366 estimated by the previous simplified method and plotted with solid lines in Figs. 6 (a)-(d). When the
367 vertical SOF $\theta_{\ln E}$ ranges from $0.1H$ to $1.0H$, the probability distribution predicted by RFEM is
368 generally consistent with that estimated by the simplified method. The increase in the standard
369 deviation of the average consolidation degree can be explained by the increase of the vertical SOF
370 $\theta_{\ln E}$ in the variance function.

371 The statistics of average consolidation degree at 2×10^6 s and 1×10^7 s are separately calculated

by RFEM and the simplified method. The results are summarized in Table 3. As the $\theta_{\ln E}$ ranges from 0.1H to 1.0H, the mean value of the average consolidation degree varies little, indicating that the mean values of the average consolidation degree are independent of the vertical SOF of Young modulus. The maximum relative difference $\delta_{\max}$ is less than 5%, which means that the mean values of the average consolidation degree of the two methods are in good agreement. However, the vertical SOF has a significant influence on the standard deviation of the average consolidation degree. It can be seen from Table 3 that the standard deviation of the average consolidation degree increases with the increase of $\theta_{\ln E}$. On the whole, the maximum relative difference $\delta_{\max}$ of the variances predicted by the two methods is less than 15% and approximately equal. In the extreme case of large $\theta_{\ln E}$, the standard deviation estimated by the simplified method is approximate to RFEM. In this case, Young modulus tends to the same value in an anisotropic random field that can be considered as a random variable, and the value of the variance function is approximately equal to 1.0. Therefore, the standard deviations obtained by these two methods are very close when $\theta_{\ln E}$ takes a large value.

The curves of the statistics of the average consolidation degree over time are plotted in Figs. 7 (a) and (b), as obtained from a number of RFEM simulations. The mean value of the average consolidation degree increases nonlinearly with consolidation time and is not affected by the SOF of the Young modulus. With the increase of the SOF, the variance function decreases, leading to a decrease in the standard deviation of the average consolidation degree. The standard deviation first increases, and then decreases with time. As for various SOFs of Young modulus, the maximum deviations appear almost at the same time.

COV of Young modulus

The statistics of the average consolidation degree are calculated by RFEM and the simplified method, where the vertical SOF $\theta_{\ln E}$=0.2H (4m), and the COV in the range of 0.15 to 0.30. The

results are listed in Table 4. The mean value of the average consolidation degree calculated by the simplified method is in good agreement with that calculated by RFEM within the specified COV of Young modulus. However, it can be seen from Table 4 that COV has an obvious influence on the standard deviation of the average consolidation degree. When the COV doubles from 0.15 to 0.30, the standard deviation of the average consolidation degree almost doubles. The relative difference of the average consolidation degrees calculated by the two methods is less than 15%, indicating the effectiveness of the simplified method.

According to the results, the horizontally stratified anisotropic random field is an effective and accurate tool to describe the spatial variability of soil. As the COV or vertical SOF of the anisotropic random field of Young modulus increases, the mean value of the average consolidation degree changes very little, while the standard deviation rises rapidly. Additionally, to avoid a number of RFEM simulations in practical engineering, the simplified method is suggested to estimate the probability distribution of consolidation settlement within the allowable error.

As can be seen from Fig. 8, the COV of the Young modulus affects the mean value and standard deviation of the average consolidation degree in a similar way to the SOF. The COV of the Young modulus has almost no effect on the mean value of the average consolidation degree, while the standard deviation of the average consolidation degree increases as the COV of the Young modulus increases. The standard deviation increases first and then decreases with time. The main reason for the decrease in standard deviation is that the number of RFEM realizations that achieve complete consolidation increases gradually over time, thereby reducing the standard deviation.

4.1.2 Anisotropic random field of permeability

In order to measure the effects of permeability on consolidation, a number of RFEM realizations

419 are performed, where permeability is represented by anisotropic random field and Young modulus
420 is a constant value, as listed in Table 1. For the given vertical SOF $\theta_{\ln k}$ and COV of permeability, the
421 average consolidation degree at any consolidation time is evaluated by RFEM.

422 *Vertical SOF of permeability*
423

424 The probability distributions of average consolidation degree obtained by RFEM are plotted with
425 histograms and dotted lines, as shown in Figs. 9 (a)-(d). The results indicate that when the vertical
426 SOF $\theta_{\ln k}$ is large, the average consolidation degree is widely dispersed. Furthermore, for $\theta_{\ln k}=1.0H$
427 and COV=3.0, the average consolidation degree of some RFEM realizations reaches 1.0, indicating
428 the completion of consolidation. Moreover, the probability of complete consolidation increases
429 gradually with time. Therefore, there are two peaks in the probability distribution of Fig. 9 (d).

430 In an extreme case, when $\theta_{\ln k}$ is large enough, each variable in the random field of permeability
431 approximates a constant value. That is to say, permeability can reasonably be regarded as a random
432 variable. Through the reasoning similar to section 4.1.1, the permeability is taken as a random
433 variable to derive the probability distribution of the average consolidation degree, which is given by
434 Eq. (18). Then, the variance function in Eq. (9) is used to consider the effect of vertical SOF. Finally,
435 the probability distribution is recalculated according to the reduced standard deviation.

436 $$f(U)=\frac{k}{2T_v\sum_{m=1}^{\infty}e^{-M^2T_v}}f(k) \tag{18}$$

437 The probability distributions of average consolidation degree estimated by the previous
438 simplified method are plotted with solid lines, and the statistics are shown in Fig. 9. The results show
439 that as the $\theta_{\ln k}$ increases, the mean value and standard deviation increase, and the probability
440 distribution evaluated by the simplified method gradually approaches that obtained by RFEM. When

441 the $\theta_{\ln k}$ is greater than 10 m, the probability distribution obtained by RFEM is approximately equal
442 to that obtained by the simplified method.

443 Table 5 shows the statistics of the average consolidation degree at 2×10^6 s and 1×10^7 s for $\theta_{\ln k}$ in
444 the range of 0.1~1.0H. As can be seen from Table 5, there are large differences in the statistics of
445 average consolidation degree at 1×10^7 s for a small value of $\theta_{\ln k}$. From the perspective of the spatial
446 variability, low permeability soils bunched together are not conducive to drainage when $\theta_{\ln k}$ takes a
447 small value. Since the blockage effect (the so-called blockage effect is first presented by Huang *et al.*
448 2010) is not taken into account, the simplified method overestimates the mean value of the average
449 consolidation degree and underestimates its standard deviation. This is why there is a large
450 difference between the two approaches.

451 To better understand the influence of the vertical SOF $\theta_{\ln k}$ on consolidation, the curves of the
452 statistics of the average consolidation degree over time calculated by RFEM are shown in Fig. 10.
453 The mean value increases with time, while the standard deviation increases at first and then
454 decreases with time. As shown in Figs. 10 (a)-(b), $\theta_{\ln k}$ of the anisotropic random field of permeability
455 has little influence on the mean value, but a significant influence on the standard deviation. As the
456 $\theta_{\ln k}$ increases, the variance function of the consolidated soil increases, resulting in a large variability
457 of the average consolidation degree. It is worth noting that the standard deviation begins to decrease
458 almost at the same time for various $\theta_{\ln k}$.

459 *COV of permeability*
460

461 From the above analysis, it can be seen that due to the blocking effect caused by the vertical SOF
462 of permeability, the calculation results of the simplified method have a large error. Therefore, the
463 statistics of the average consolidation degree are calculated by using RFEM. As for various COVs,

464 the statistics of the average consolidation degree over time are plotted in Figs. 11 (a)-(b), in which
465 $\theta_{\ln k}$ takes $0.2H$. As shown in Fig. 11 (a), the mean value of the average consolidation degree increases
466 with time. As the COV of the permeability increases from 1.0 to 3.0, the time required to complete
467 consolidation is prolonged. The blockage effect caused by bunched regions with low permeability
468 soil is more obvious for a greater value of COV, which results in more time to complete consolidation.
469 The curves shown in Fig. 11 (b) indicate that the standard deviation of the average consolidation
470 degree increases with time, and then eventually decreases. For the anisotropic random fields of
471 permeability with larger COV, the blockage effect is more likely to occur and the time to complete
472 consolidation is prolonged. At the later stage, some RFEM realizations have been fully consolidate
473 with the average consolidation degrees reaching 1.0, thus reducing the standard deviation over time.
474 In fact, as the COV increases, the reduction of the standard deviation is delayed, which means the
475 COV of permeability has an obvious influence on the consolidation process.
476
477 *4.2 Influence of anisotropic random field on creep deformation*
478 *4.2.1 Convergence and probabilistic analysis of creep deformation*
479 In the RFEM simulation for creep deformation, the anisotropic random field with specified SOF
480 and COV illustrated in section 3.2.2 is used to consider the spatial variability of the secondary
481 consolidation coefficient. According to the results of RFEM, one worse case of convergence,
482 $\theta_{\ln C\alpha e}$=4 m, and COV=0.2, is chosen to determine a reasonable number of RFEM simulations. The
483 creep time in this analysis ranges from 30 days to 360 days. The curves of the standard deviation of
484 creep deformation with respect to the number of RFEM realizations are shown in Fig. 12. The
485 horizontal axis and the vertical axis represent the number of RFEM realizations and the standard
486 deviation of creep deformation, respectively. It can be seen that the standard deviation remains stable

after 600 RFEM realizations, which indicates the convergence of the RFEM realization. In view of the computational efficiency, the optimal number of RFEM realizations is 600, and it is adopted in the following analysis.

The possible creep deformations are obtained from 600 RFEM realizations with the secondary consolidation coefficient as the anisotropic random field. According to the simulation results, probability distributions of creep deformation at different times are depicted in Fig. 13, where $\theta_{\ln C\alpha e}$=4m, COV=0.2. As the creep progresses, the mean value and standard deviation of creep deformation increase gradually. The results reveal that the creep deformation gradually diverges over time, which means that the uncertainty of the creep deformation gradually accumulates at the same time.

4.2.2 SOF of secondary consolidation coefficient

The possible creep deformations within 30 years are calculated by RFEM, and the COV of the secondary consolidation coefficient is 0.2. The mean value and standard deviation of creep deformation for various vertical SOFs $\theta_{\ln C\alpha e}$ are shown in Fig. 14.

As shown in Figs. 14 (a)-(b), the mean value and standard deviation of creep deformation increase nonlinearly with time. After 30 years of creep, the mean value and standard deviation remain almost constant, and their maximum values reach 0.65 m and 0.14 m, respectively. The results show that the vertical SOF $\theta_{\ln C\alpha e}$ has little effect on the mean value of creep deformation but an obvious effect on its standard deviation, which is consistent with the effect of Young modulus' SOF on the foundation deformation investigated by Fenton and Griffiths (2002). It is easy to find from Fig. 14 (b) that the standard deviation of creep deformation is positively correlated with $\theta_{\ln C\alpha e}$. In fact, the generality variance of the secondary consolidation coefficient along the depth of soil

increases with the increase of $\theta_{\ln Cae}$, which in turn leads to an increase in the standard deviation of creep deformation.

In order to better explain the creep deformation range for various $\theta_{\ln Cae}$, 99.7% confidence intervals are estimated by the results of RFEM. Fig. 15 presents the curves of upper and lower limits of creep deformation with respect to time when the confidence level is 99.7%. For the same $\theta_{\ln Cae}$, the curves of the upper and lower limits are drawn with the same line type. The interval between upper limit and the lower limit represents the confidence interval of creep deformation. The confidence interval gradually increases with creep time and $\theta_{\ln Cae}$. Even for different $\theta_{\ln Cae}$, the confidence interval of creep deformation remains stable almost at the same time.

4.2.3 COV of secondary consolidation coefficient

Fig. 16 shows the mean value and standard deviation of the creep deformation for various COVs of the secondary consolidation coefficient, where the vertical SOF of the secondary consolidation coefficient takes 4 m. As shown in Fig. 16 (a), the mean value of creep deformation increases nonlinearly with time, and the maximum value is 0.64 m. When the COV of the secondary consolidation coefficient is in the range of 0.2 to 0.4, there is almost no difference between the mean values. It can be seen from Fig. 16 (b) that the standard deviation of creep deformation increases with time. Under the same creep time, the standard deviation increases as the COV of the secondary consolidation coefficient increases. The mean value and standard deviation of creep deformation gradually stabilize over time. After 30 years of creep, the maximum standard deviation reaches 0.11 m, which is an unacceptable and unallowable deformation for subgrades or other structures.

Fig. 17 presents the upper and lower limits of creep deformation with respect to time at a 99.7% confidence level. For the same COV, the curves of the upper and lower limits are plotted with the

same line type. The confidence interval of creep deformation increases with time and then remains constant. In addition, the dispersion of creep deformation increases with the increase of COV.

From the results shown in Fig. 15 and Fig. 17, it seems impossible to accurately estimate the creep deformation of spatial variability clay soils by traditional deterministic approaches. However, it is interesting that after years of creep, the mean value of creep deformation and the confidence interval with a confidence level of 99.7% remain constant. Therefore, if the soil has undergone a long-term creep and the creep deformation does not increase anymore, the spatial variability of the secondary consolidation coefficient can be ignored in this situation.

5. Conclusions

The spatial variability of soil properties plays a significant role in the time-dependent deformation. In this study, the probabilistic characteristics of consolidation and creep have been investigated by RFEM, in which an anisotropic random field is used to characterize the spatial variability of soil parameters. Herein, the horizontal SOF of the anisotropic random field is usually large enough in practical engineering, which means that the parameters of soil in horizontal direction remain locally unchanged. The study on the probabilistic time-dependent deformation of clay soil is beneficial to the engineering practice, and provides insightful clues to the time-dependent reliability of the engineering design. According to the results of the above-mentioned analysis, the following conclusions can be drawn.

- The vertical SOF or COV of Young modulus has little influence on the mean value of the average consolidation degree, but its standard deviation will increase as the vertical SOF or COV increases. Compared to RFEM, the simplified method considering the spatial variability of the Young modulus is efficient to estimate the consolidation.

- The vertical SOF of permeability has little influence on the mean value of the average consolidation degree. However, the mean value decreases with an increase of COV because of the blockage effect induced by bunched regions of low permeability soil. The standard deviation of the average consolidation degree increases at first and then decreases. The larger value of the SOF or COV leads to a higher dispersion in the average consolidation degree.
- The spatial variability of permeability causes a blockage effect, which makes the simplified method overestimate the mean value of the average consolidation degree, and underestimate its standard deviation.
- Considering the anisotropic random field of secondary consolidation coefficient, the creep deformation increases with time and then tends to a constant value. Meanwhile, the uncertainty of creep deformation gradually accumulates and finally remains unchanged.
- The vertical SOF and COV of the anisotropic random field of secondary consolidation coefficient have little influence on the mean value of creep deformation, but a great influence on its standard deviation. Additionally, the variability of creep deformation increases gradually with an increase in vertical SOF or COV.

Acknowledgments

The research described in this paper is substantially supported by the National Natural Science Foundation of China (No. 51538009 and No. 51778474). Hereby, the authors are grateful to these programs.

References

Baecher, G.B., Christian, J.T. (2003), Reliability and Statistics in Geotechnical Engineering. John Wiley and Sons Ltd.

Bárdossy, G. and Fodor, J. (2001), "Traditional and new ways to handle uncertainty in geology", *Natural Resources Research*, **10**(3):179-187. https://doi.org/10.1023/a:1012513107364.

Benson, C.H. (1993), "Probability distributions for hydraulic conductivity of compacted soil liners", *Journal of Geotechnical Engineering*, **119**(3), 471-486. https://doi.org/10.1061/(ASCE)0733-9410(1993)119:3(471).

Bergman, L.A., Shinozuka, M. and Bucher, C.G. (1997), "A state-of-the-art report on computational stochastic mechanics", *Probabilistic Engineering Mechanics*, **12**(4), 197-321. https://doi.org/10.1016/S0266-8920(97)00003-9.

Biot, M.A. (1941), "General theory of three-dimensional consolidation", *Journal of Applied Physics*, **12**(2), 155-164. https://doi.org/10.1063/1.1712886.

Bong, T. and Stuedlein, A.W. (2018), "Efficient methodology for probabilistic analysis of consolidation considering spatial variability", *Engineering Geology*, **237**, 53-63. https://doi.org/10.1016/j.enggeo.2018.02.009.

Casagrande, A. (1936), "The determination of pre-consolidation load and its practical significance". *Proc. of Fist ICMFE*, **3**, 60-64.

Chenari, R.J., Fatahi, B., Ghoreishi, M. and Taleb, A. (2019), "Physical and numerical modelling of the inherent variability of shear strength in soil mechanics", *Geomechanics and Engineering*. **17**(1), 31-45. https://doi.org/10.12989/gae.2019.17.1.031.

Cho, S.E. (2010), "Probabilistic assessment of slope stability that considers the spatial variability of soil properties", *Journal of Geotechnical & Geoenvironmental Engineering*, **136**(7), 975-984. https://doi.org/10.1061/(ASCE)GT.1943-5606.0000309.

Fei, S.Z., Tan, X.H., Wang, X., Du, L.F. and Sun, Z.H. (2019), "Evaluation of soil spatial variability by micro-structure simulation", *Geomechanics and Engineering*, **17**(6), 565-572. https://doi.org/10.12989/gae.2019.17.6.565.

Fenton, G.A. and Griffiths, D.V. (2002), "Probabilistic foundation settlement on spatially random soil", *Journal of Geotechnical & Geoenvironmental Engineering*, **128**(5), 381-390. https://doi.org/10.1061/(ASCE)1090-0241(2002)128:5(381).

Hu, B. and Schiehlen, W. (1997), "On the simulation of stochastic processes by spectral representation", *Probabilistic Engineering Mechanics*, **12**(2), 105-113. https://doi.org/10.1016/S0266-8920(96)00039-2.

Huang, H.W., Xiao, L., Zhang, D.M. and Zhang, J. (2017), "Influence of spatial variability of soil Young's modulus on tunnel convergence in soft soils", *Engineering Geology*, **228**, 357-370. https://doi.org/10.1016/j.enggeo.2017.09.011.

Huang, J., Griffiths, D.V. and Fenton, G.A. (2010), "Probabilistic analysis of coupled soil consolidation", *Journal of Geotechnical and Geoenvironmental Engineering*, **136**(3), 417-430. https://doi.org/10.1061/(ASCE)GT.1943-5606.0000238.

Karim, M.R. and Gnanendran, C.T. (2014), "Review of constitutive models for describing the time dependent behaviour of soft clays", *Geomechanics & Geoengineering*, **9**(1), 36-51. https://doi.org/10.1080/17486025.2013.804212.

Kim, D., Ryu D., Lee C., et al. (2013), "Probabilistic evaluation of primary consolidation settlement of Songdo New City by using kriged estimates of geologic profiles", *Acta Geotechnica*, 2013, **8**(3), 323-334. https://doi.org/10.1007/s11440-012-0192-5.

Lee, I.K., White, W. and Ingles, O.G. (1983), Geotechnical Engineering, Pitman, London.

Li, X.Y. and Hu, L.Q. (2011), "Probabilistic analysis of one-dimensional consolidation with Monte Carlo simulations", *Applied Mechanics & Materials*, **55-57**, 907-912. https://doi.org/10.4028/www.scientific.net/AMM.55-57.907.

Morsy, M.M., Morgenstern, N.R. and Chan, D.H. (1995), "Simulation of creep deformation in the foundation

of Tar Island Dyke", *Canadian Geotechnical Journal*, **32**(6), 1002-1023. https://doi.org/10.1139/t95-098.
Papaioannou, I. and Straub, D. (2012), "Reliability updating in geotechnical engineering including spatial variability of soil". *Computers and Geotechnics*, **42**, 44-51. https://doi.org/10.1016/j.compgeo.2011.12.004.
Phoon, K.K. and Kulhawy, F.H. (1999), "Characterization of geotechnical variability", *Canadian Geotechnical Journal*, **36**(4), 612-624. https://doi.org/10.1139/t99-038.
Prevost, J.H., Deodatis, G. and Popescu, R. (1997), "Effects of spatial variability on soil liquefaction: some design recommendations", *Géotechnique*, **47**(5), 1019-1036. https://doi.org/10.1680/geot.1997.47.5.1019.
Rehfeldt K.R., Boggs J.M. and Gelhar L.W. (1992), "Field study of dispersion in a heterogeneous aquifer: 3. Geostatistical analysis of hydraulic conductivity", *Water Resources Research*, **28**(12), 3309-3324. https://doi.org/10.1029/92WR01758.
Stefanou, G. (2009), "The stochastic finite element method: Past, present and future", *Computer Methods in Applied Mechanics and Engineering*, 2009, **198**(9-12), 1031-1051. https://doi.org/10.1016/j.cma.2008.11.007.
Vanmarcke, E.H. (2010), Random Fields: Analysis and Synthesis (Revised and Expanded), World Scientific Publishing Co. Pte. Ltd., Singapore.
Xu, S., Chen, Y.L. and Zhao, C.X. (2008), "One-dimensional consolidation tests of creep deformation and secondary consolidation characteristics of soft soil in Shanghai area", *Journal of Engineering Geology*, **16**(4), 495-501. https://doi.org/10.3969/j.issn.1004-9665.2008.04.010.
Yin, Z.Y., Chang, C.S., Karstunen, M. and Hicher, P.Y. (2010), "An anisotropic elastic–viscoplastic model for soft clays", *International Journal of Solids and Structures*, **47**(5), 665-677. https://doi.org/10.1016/j.ijsolstr.2009.11.004.
Zhang, L.L., Zhang, L .M. and Tang, W.H. (2005), "Rainfall-induced slope failure considering variability of soil properties", *Géotechnique*, **55**(2), 183-188. https://doi.org/10.1680/geot.2005.55.2.183.

Table lists

Table 1 Basic statistics of soil consolidation parameters (Baecher and Christian 2003, Benson 1993).
Table 2 Physical parameters for creep model (Yin *et al.* 2010, Xu *et al.* 2008).
Table 3 Statistics estimated by RFEM and simplified method for different SOFs of Young modulus (μ=10 kPa, COV = 0.2).
Table 4 Statistics estimated by RFEM and the simplified method for different COVs of Young modulus (μ =10 kPa, $\theta_{\ln E} = 0.2H$).
Table 5 Statistics estimated by RFEM and the simplified method for various SOFs of permeability (μ=10^{-7}m/s, COV = 1.0).

Table 1 Basic statistics of soil consolidation parameters (Baecher and Christian 2003, Benson 1993)

	μ	COV	Horizontal SOF	Vertical SOF
E	10 kPa	0.2	40 m	4 m
k	10^{-7} m/s	1.0	40 m	4 m

Table 2 Physical parameters for creep model (Yin *et al.* 2010, Xu *et al.* 2008)

λ	κ	e_0	υ	M_c	P_0	k	$C_{\alpha e}$
0.197	0.042	1.5	0.35	1.23	5.0kPa	10^{-8} m/s	0.006

Table 3 Statistics estimated by RFEM and simplified method for different SOFs of Young modulus (μ=10 kPa, COV = 0.2)

$\theta_{\ln E}$	μ_{vt20}	μ_{vt100}	$\hat{\mu}_{vt20}$	$\hat{\mu}_{vt100}$	δ	σ_{vt20}	σ_{vt100}	$\hat{\sigma}_{vt20}$	$\hat{\sigma}_{vt100}$	δ
	RFEM		Simplified method			RFEM		Simplified method		
0.1H	0.31	0.68	0.32	0.69	0.03	0.011	0.019	0.010	0.018	0.10
0.2H	0.31	0.69	0.32	0.69	0.03	0.016	0.027	0.014	0.025	0.14
0.5H	0.31	0.69	0.32	0.69	0.03	0.023	0.041	0.020	0.038	0.15
1.0H	0.32	0.69	0.32	0.69	0.00	0.026	0.050	0.026	0.048	0.04

Hereby, $\delta_{\max}$ refers to the maximum relative difference, which is defined by the ratio of the maximum difference between the average consolidation degrees calculated by RFEM and the simplified method to that obtained by RFEM.

Table 4 Statistics estimated by RFEM and the simplified method for different COVs of Young modulus (μ =10 kPa, $\theta_{\ln E} = 0.2H$)

COV	μ_{vt20}	μ_{vt100}	$\hat{\mu}_{vt20}$	$\hat{\mu}_{vt100}$	δ	σ_{vt20}	σ_{vt100}	$\hat{\sigma}_{vt20}$	$\hat{\sigma}_{vt100}$	δ
	RFEM		Simplified method			RFEM		Simplified method		
0.15	0.31	0.69	0.32	0.70	0.03	0.011	0.020	0.010	0.019	0.10
0.20	0.31	0.69	0.32	0.69	0.03	0.016	0.027	0.014	0.025	0.14
0.25	0.31	0.68	0.32	0.69	0.03	0.019	0.033	0.017	0.032	0.12
0.30	0.31	0.67	0.31	0.69	0.00	0.023	0.040	0.020	0.038	0.15

Table 5 Statistics estimated by RFEM and the simplified method for various SOFs of permeability (μ=10^{-7} m/s, COV = 1.0)

$\theta_{\ln k}$	μ_{vt20}	μ_{vt100}	$\hat{\mu}_{vt20}$	$\hat{\mu}_{vt100}$	δ	σ_{vt20}	σ_{vt100}	$\hat{\sigma}_{vt20}$	$\hat{\sigma}_{vt100}$	δ
	RFEM		Simplified method			RFEM		Simplified method		
0.1H	0.17	0.32	0.18	0.41	0.28	0.068	0.114	0.044	0.097	0.35
0.2H	0.19	0.35	0.19	0.42	0.20	0.089	0.144	0.064	0.135	0.28
0.5H	0.22	0.42	0.20	0.44	0.05	0.124	0.202	0.105	0.197	0.15
1.0H	0.22	0.44	0.22	0.45	0.02	0.150	0.241	0.143	0.238	0.05

Figure lists

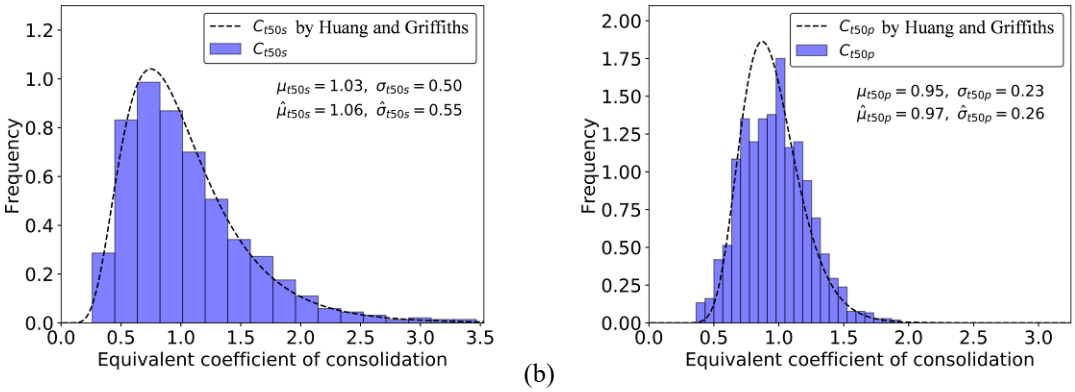

Fig. 1 Probability distributions of the equivalent consolidation coefficient, (a) C_{t50s} calculated by settlement, (b) C_{t50p} calculated by excess pore pressure.

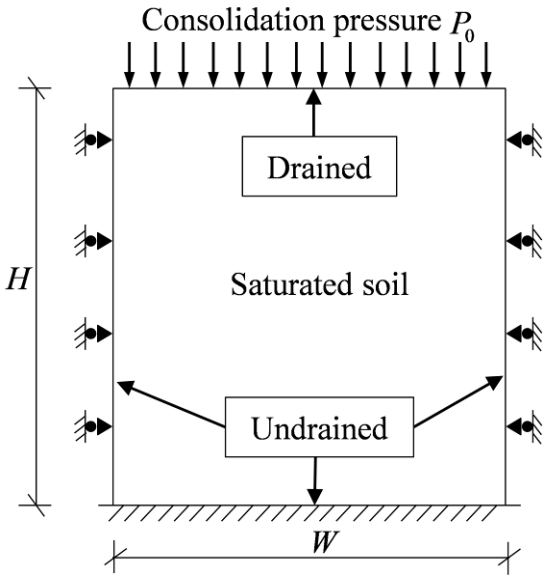

Fig. 2 Physical model of RFEM for the time-dependent deformation.

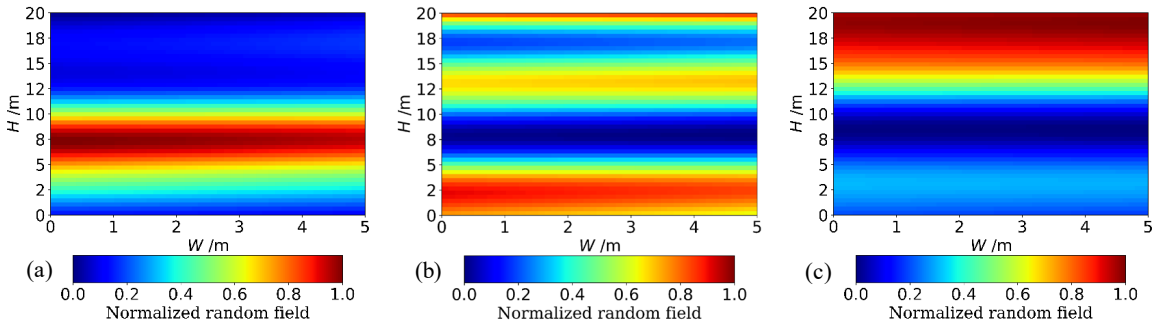

Fig. 3 Realizations of normalized anisotropic random field (vertical SOF=4 m), (a) horizontal SOF=20 m, (b) Horizontal SOF=50 m, (c) Horizontal SOF=80 m.

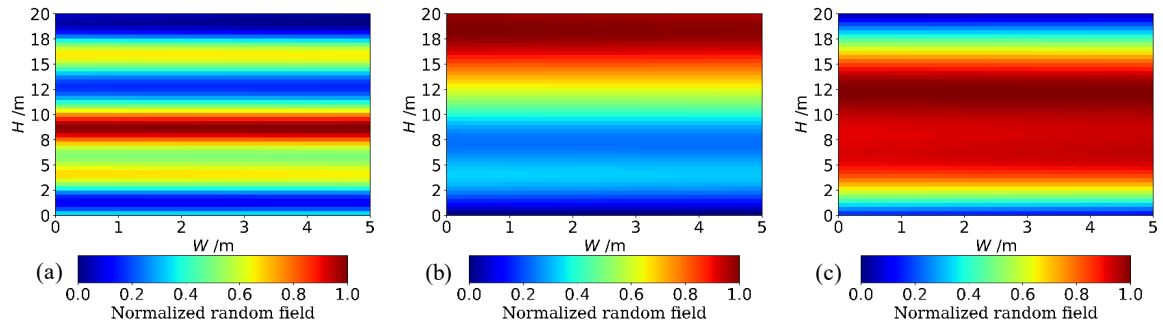

Fig. 4 Realizations of the normalized anisotropic random field (horizontal SOF=50 m), (a) vertical SOF=2 m, (b) vertical SOF=4 m, (c) vertical SOF=6 m.

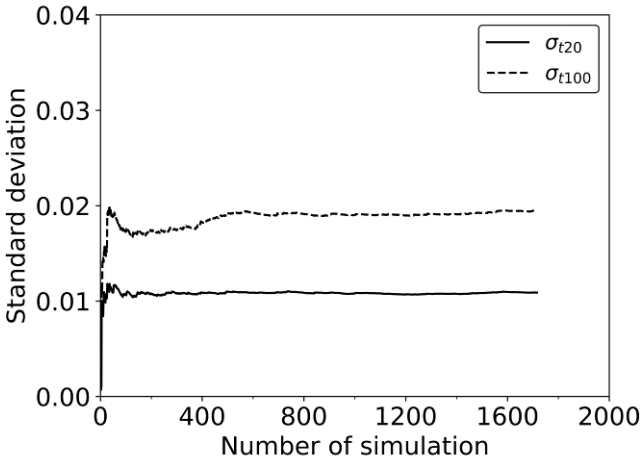

Fig. 5 Convergence of the RFEM realization for the average consolidation degree.

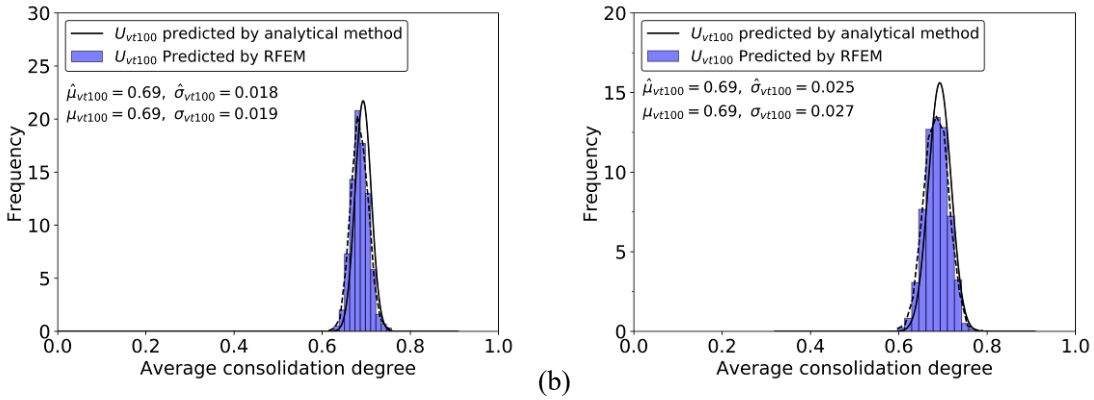

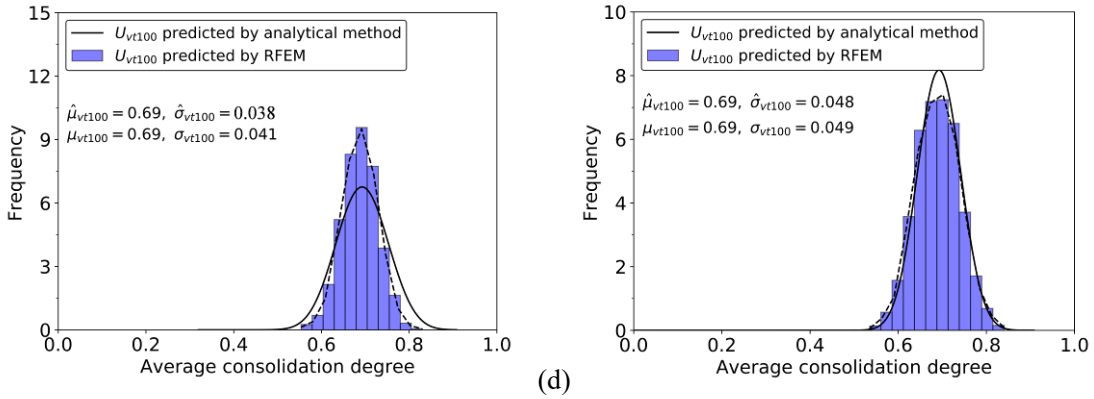

(c) (d)

Fig. 6 Probability distributions of the average consolidation degree for different $\theta_{\ln E}$ ($t = 10^7$ s, $\mu = 10$ kPa, $COV = 0.2$), (a) $\theta_{\ln E} = 0.1H$, (b) $\theta_{\ln E} = 0.2H$, (c) $\theta_{\ln E} = 0.5H$, (d) $\theta_{\ln E} = 1.0H$.

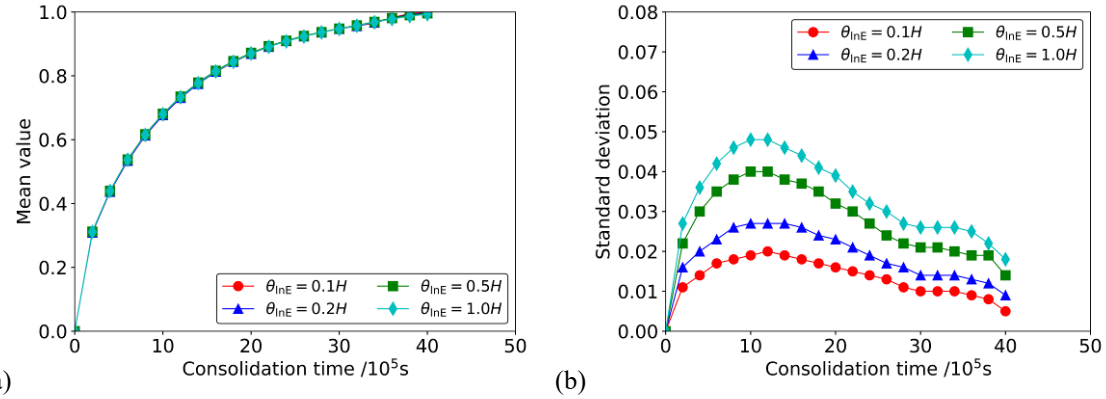

(a) (b)

Fig. 7 Curves of the statistics of the average consolidation degree with time for various SOFs of Young modulus ($\mu = 10$ kPa, $COV = 0.2$), (a) mean value, (b) standard deviation.

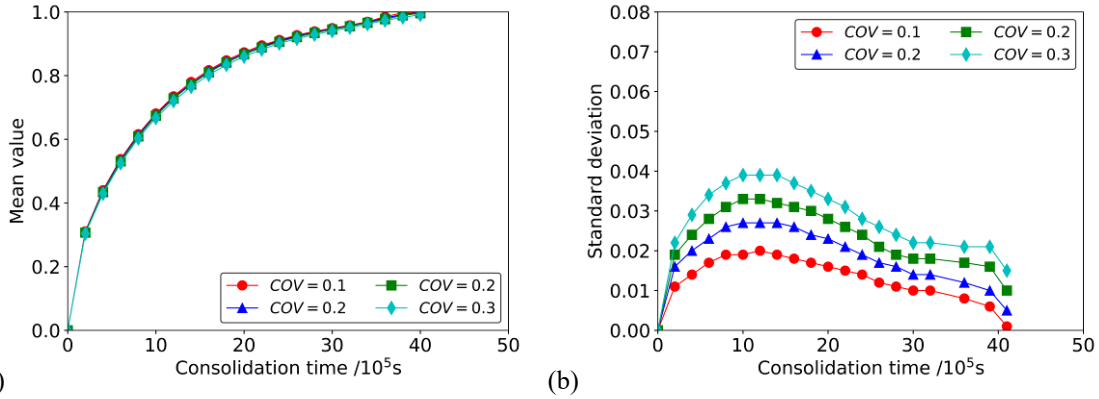

(a) (b)

Fig. 8 Curves of the statistics of average consolidation degree with time for various COVs of Young modulus ($\mu = 10$ kPa, $\theta_{\ln E} = 0.2H$), (a) mean value, (b) standard deviation.

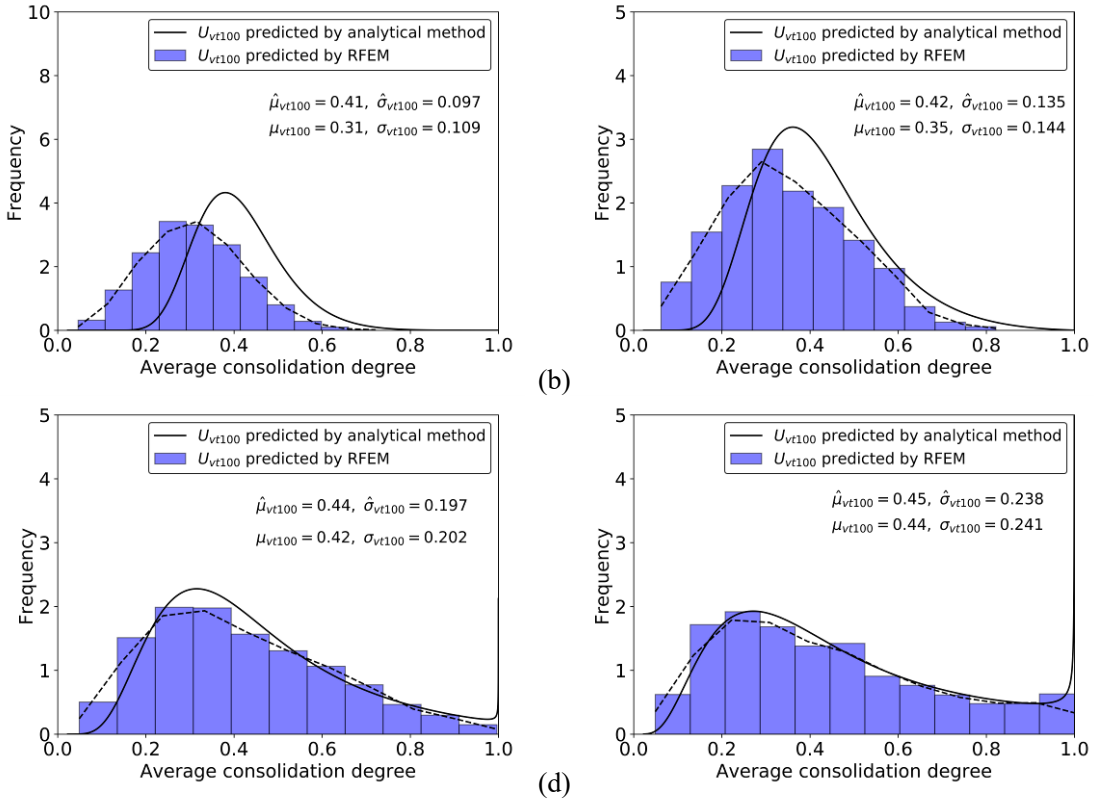

Fig. 9 The probability distributions of average consolidation degree for various SOFs of permeability (t = 10^7 s, μ=10^{-7} m/s, COV = 1.0), (a) $\theta_{\ln k}$=0.1H, (b) $\theta_{\ln k}$=0.2H, (c) $\theta_{\ln k}$=0.5H, (d) $\theta_{\ln k}$=1.0H.

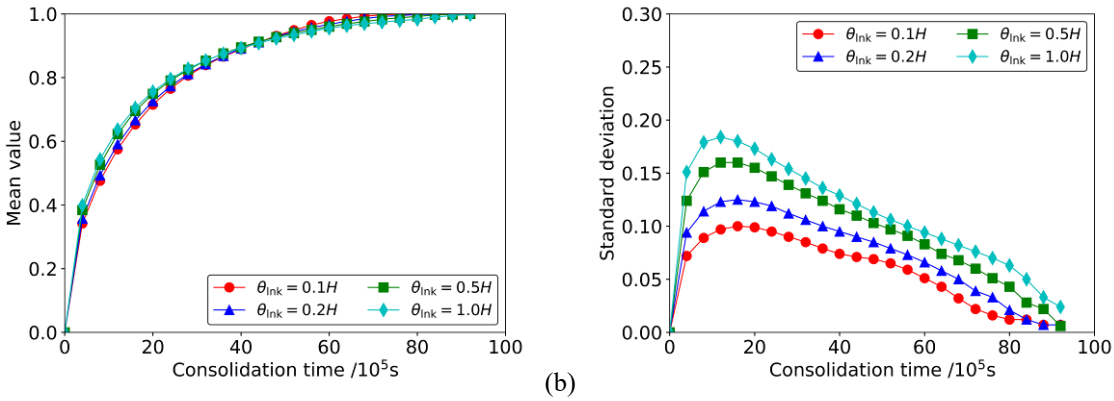

Fig. 10 Curves of the statistics of average consolidation degree with time for various SOFs of permeability (μ=10^{-7} m/s, COV = 1.0), (a) mean value, (b) standard deviation.

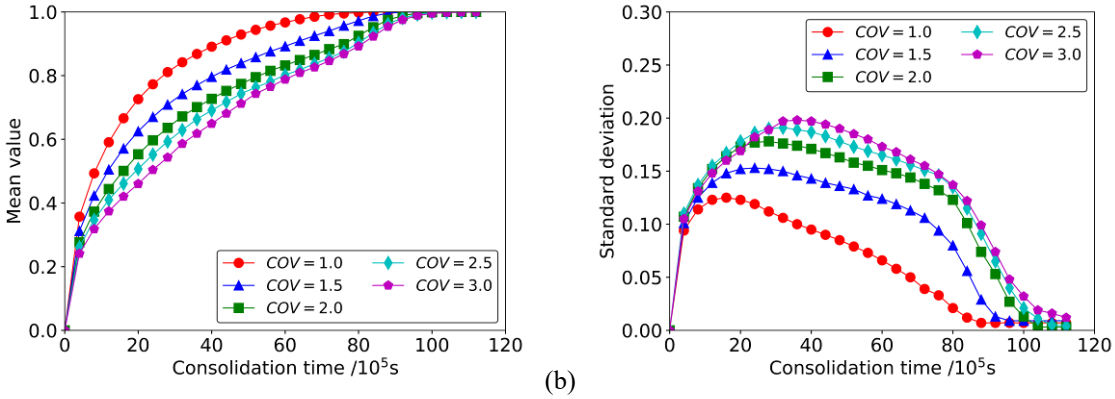

(a) (b)

Fig. 11 Curves of the statistics of average consolidation degree with time for various COVs of permeability (μ=10^{-7} m/s, $\theta_{\ln k} = 0.2H$), (a) mean value, (b) standard deviation.

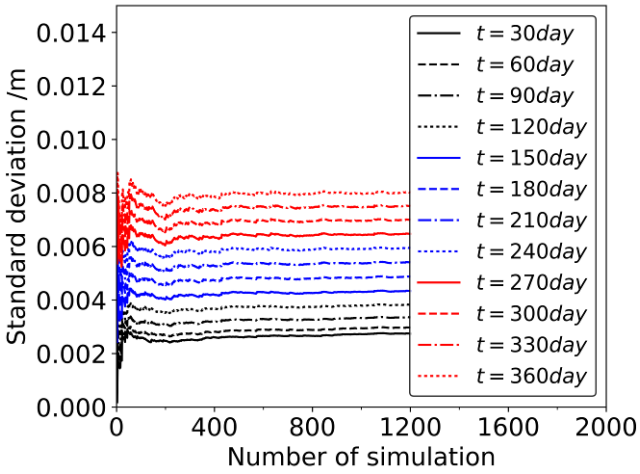

Fig. 12 Convergence of the RFEM realization for the creep deformation ($\theta_{\ln Cae}$=4 m, COV=0.2).

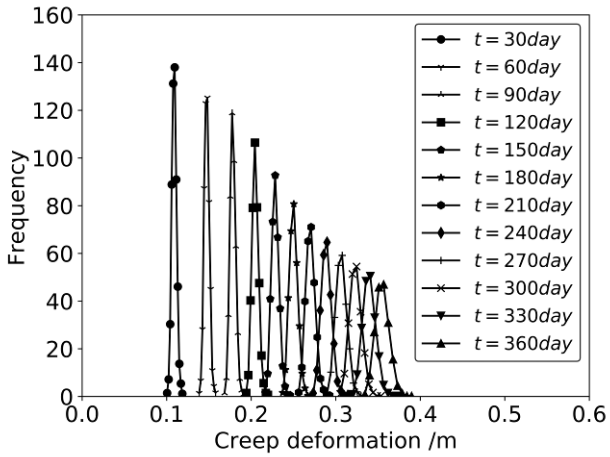

Fig. 13 Probability distributions of creep deformation at different times ($\theta_{\ln Cae}$=4 m, COV=0.2).

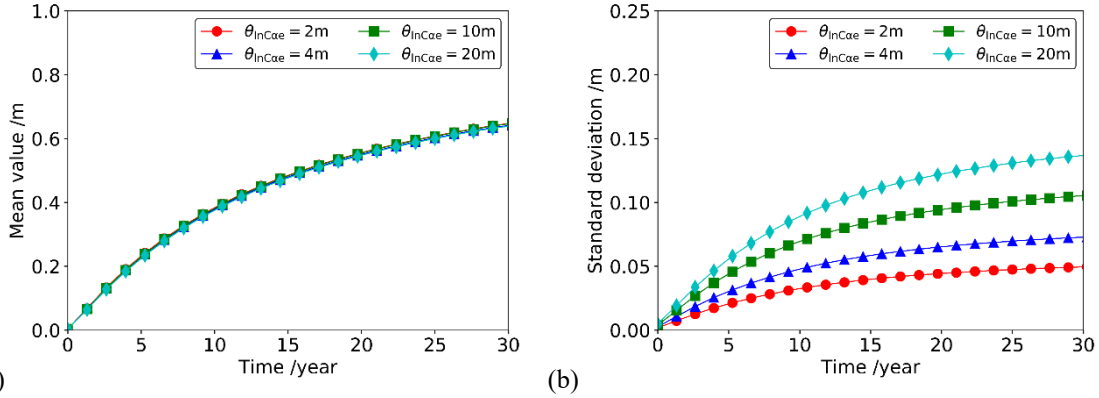

(a) (b)

Fig. 14 Time-varying statistics of creep deformation for various SOFs of secondary consolidation coefficient (μ=0.006, COV = 0.2), (a) mean value, (b) standard deviation.

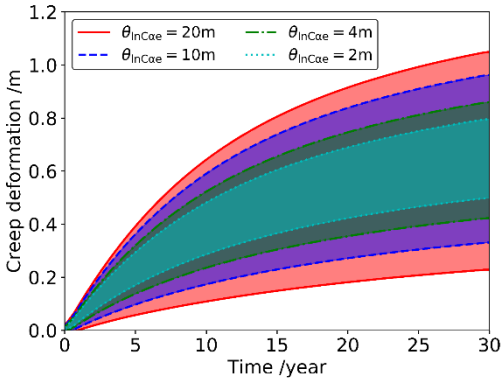

Fig. 15 99.7% confidence interval of creep deformation for various SOFs of secondary consolidation coefficient (μ=0.006, COV = 0.2).

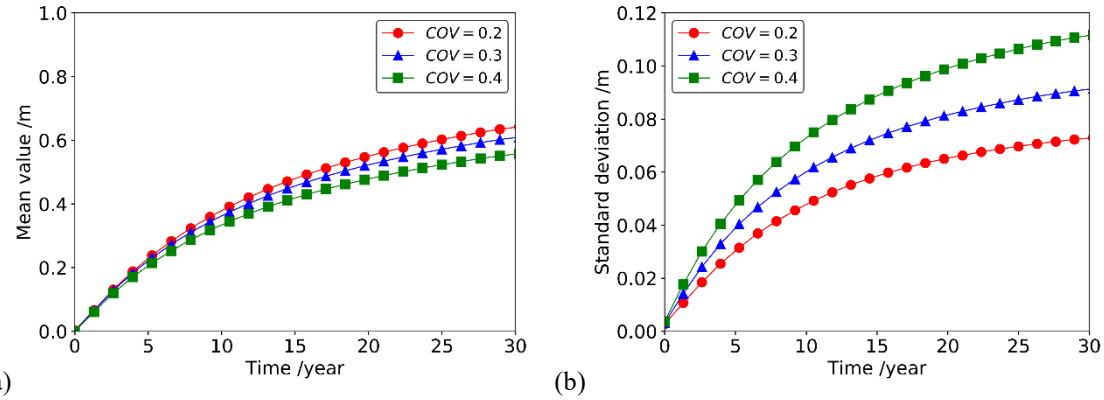

(a) (b)

Fig. 16 Time-varying statistics of creep deformation for various COVs of secondary consolidation

coefficient (μ=0.006, $\theta_{\ln Cae}$ = 4 m), (a) mean value, (b) standard deviation.

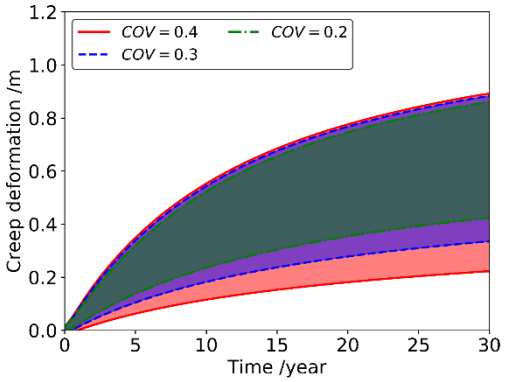

Fig. 17 99.7% confidence interval of creep deformation for COVs of secondary consolidation coefficient (μ=0.006, $\theta_{\ln Cae}$ = 4 m).